

COOMET Supplementary Comparison**(Bilateral comparison between VNIIOFI, Russia and NIST, USA)****COOMET.PR-S7****Laser Power Responsivity****(COOMET Project 599/RU/13)****Final Report****17 September 2020**

Sergey A. Moskalyuk¹, Anatoly A. Liberman¹, Joshua Hadler², Paul Williams²

¹ *Federal State-Owned Unitary Enterprise “All-Russian Research Institute for Optical and Physical Measurements” (VNIIOFI), 119361, Russia, Moscow, Ozernaia str., 46*

² *National Institute of Standards and Technology. Applied Physics Division, 325 Broadway, Boulder, CO 80305*

Contents

1. Introduction	3
2. Organization	3
3. Description of artefacts	4
4. Measurement at VNIIOFI	5
5. Measurement at NIST	11
6. Results	13
7. Conclusions	18

1. Introduction

The National Institute of Standards and Technology (NIST) and the All-Russian Research Institute for Optical and Physical Measurements (VNIIOFI) agreed in February 2013 to conduct a bilateral comparison on the laser power responsivity at wavelengths of 532 nm, 1.064 μm and 10.6 μm . The aim of this comparison is to assess the equivalence of the laser power responsivity between two laboratories.

The 1 W comparison at 10.6 μm was outside the advertised measurement range and had to be withdrawn because it was discovered that the attenuation mechanism available at the time was not able to provide the attenuation with sufficient accuracy to support the measurement.

The comparison was conducted within the COOMET regional metrological organization (COOMET project 599/RU/13) and was registered at BIPM KCDB as a supplementary comparison with the identification COOMET.PR-S7

2. Organization

2.1. Pilot

The VNIIOFI was the pilot laboratory in the comparison among the participants.

2.2. Participants' details

NMI Name (Country)	Personnel	Contact information
NIST (USA)	Joshua Hadler	National Institute of Standards and Technology. Applied Physics Division 325 Broadway, Boulder, CO 80305, USA Phone: +1 303.497.4451
VNIIOFI (Russia)	Sergey Moskalyuk	Federal State-Owned Unitary Enterprise "All-Russian Research Institute for Optical and Physical Measurements" Department of near-monochromatic optical radiation (F-2) 119361, Russia, Moscow, Ozernaia str., 46, Phone: +7 495 437-34-47

2.3. Form of comparison

The comparison was carried out using a detector head for measuring laser power. The detector head was supplied by VNIIOFI. The comparison took the form of a double-sided type comparison. VNIIOFI calibrated the VNIIOFI detector head in August 2013 and then sent it to NIST. NIST calibrated detector head in May 2014 and then returned it to VNIIOFI. VNIIOFI recalibrated detector head to check the drift during the period in June 2015.

Detector head used: OPHIR 10A (VNIIOFI).

Therefore, the sequence of the detector measurements were the following:

For OPHIR 10A: VNIIOFI (Aug 2013) – NIST (May 2014) – VNIIOFI (June 2015)

NIST sent their measurement results to the pilot (VNIIOFI) in June 2015. VNIIOFI collected both measurement results and sent them to NIST. VNIIOFI as the pilot laboratory prepared the first version of the Draft A Report in February 2016.

3. Description of the artefacts

3.1. VNIIOFI Artefact

The VNIIOFI measurement artefact was a detector head of the Ophir 10A type (Figure 1). The thermopile sensor of the detector has a series of bimetallic junctions. A temperature difference between any two junctions causes a voltage to be formed between the two junctions. Since the junctions are in series and the «hot» junctions are always on the inner, hotter side, and the «cold» junctions are on the outer, cooler side, radial heat flow on the disc causes a voltage proportional to the power input. Laser power impinges on the center of the thermopile sensor disk (on the reverse side of the thermopile), flows radially and is cooled on the periphery. The array of thermocouples measures the temperature gradient, which is proportional to the incident or absorbed power. Since all the heat absorbed flows through the thermocouples (as long as the laser beam is inside the inner circle of hot junctions), the response of the detector is almost independent of beam size and position. If the beam is close to the edge of the inner circle, some thermocouples become hotter than others but since the sum of all of them is measured, the reading remains the same. The detector was equipped with a fixed cable. The signal voltage was measured between the Pin 9 (+) and the Pin 1 (-).

OPHIR 10A type (VNIIOFI) – Manufacturer’s specifications

Wavelength Range:	0.19 – 20 μm
Max Power:	10 W
Resolution:	1 mW
Max Avg. Power Density:	28 KW/cm ²
Max Pulse Energy Density:	2 J/cm ²
Response Time:	0.8 sec
Absorber Type:	broadband
Detector Diameter:	16 mm
Calibration Uncertainty:	$\pm 3\%$



Figure 1. Detector head of the OPHIR 10A type.

4. Measurement at VNIIOFI

4.1. Primary standard

Figure 2 shows a block scheme of the National Primary system GET 28-2013 of the unit of laser power used for the comparison.

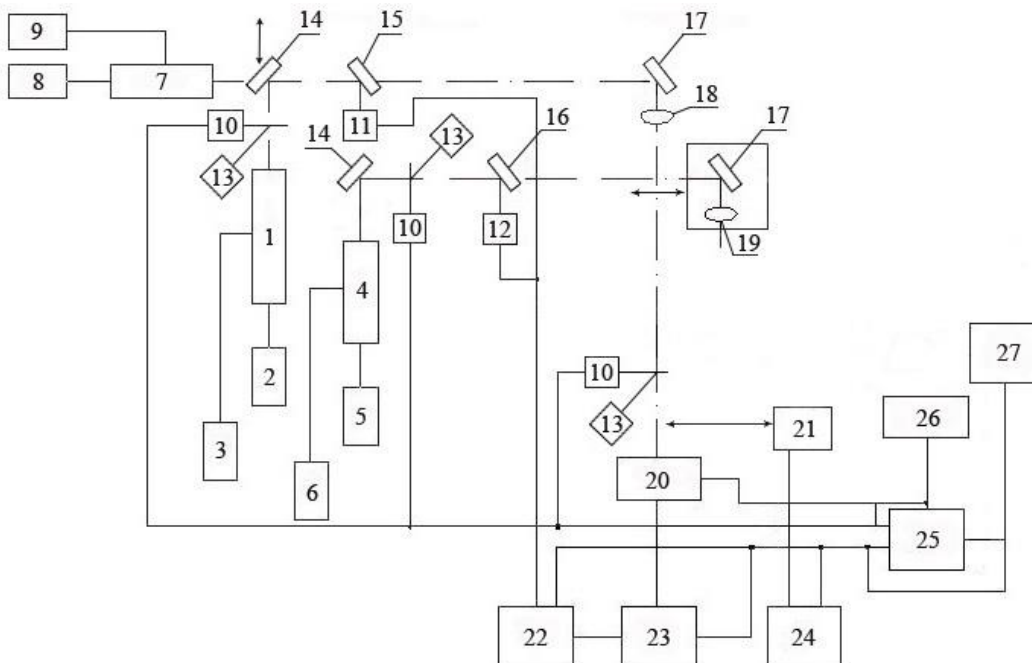


Figure 2. Block scheme of Primary standard of unit of laser power GET 28-2013.

1. Laser $\lambda=0.532 \mu\text{m}$; 2. Power module ($\lambda=0.532 \mu\text{m}$); 3. Chiller ($\lambda=0.532 \mu\text{m}$);
4. Laser $\lambda=10.6 \mu\text{m}$; 5. Power module ($\lambda=10.6 \mu\text{m}$); 6. Chiller ($\lambda=10.6 \mu\text{m}$);
7. Laser $\lambda=1.064 \mu\text{m}$; 8. Power module ($\lambda=1,064 \mu\text{m}$); 9. Chiller ($\lambda=1.064 \mu\text{m}$); 10. Shutter;
11. Monitor silicon photodiode ($\lambda=0,532 \mu\text{m}$, $\lambda=1,064 \mu\text{m}$); 12. Monitor thermophile detector ($\lambda=10,6 \mu\text{m}$); 13. Beam trap; 14. Mirror; 15. Parallel-sided plate K-8; 16. Parallel-sided plate;

17. Mirror; 18. Lens K-8; 19. Lens GaAs; 20. National Primary Standard (calorimeter PI-15) ($\lambda=0,532 \mu\text{m}$, $\lambda=1,064 \mu\text{m}$, $\lambda=10,6 \mu\text{m}$); 21. Test detector; 22. Switching unit; 23. Multimeter Keithley 2002; 24. Multimeter Agilent 34420A; 25. Control module; 26. Module for electrical calibration; 27. Computer.

Tables 4.1 and 4.2 present the lasers used in the facility and the main specifications of the primary standard.

Table 4.1 The relevant lasers that are used in GET 28-2013

Coherent Compass 1064 – 4000 M Diode – Pumped CW IR Laser (Nd: YAG)	
Wavelength	1064 nm
Power output	$\leq 4 \text{ W}$
Coherent Verdi™ V-8 Diode – Pumped Laser (Nd: YVO ₄)	
Wavelength	532 nm
Power output	$\leq 8 \text{ W}$

Table 4.2. The main specifications of the National Primary Standard (calorimeter PI-15)

Power range, W	$5 \cdot 10^{-3}$ to 2.0
Wavelengths, μm	0.532; 1.064; 10.6
Expanded uncertainty $U(k=2)$, %	0.1 (approximately)

The principle of laser power measurements is based on using a standard calorimeter with the method of substitution of optical power by electrical power. The standard calorimeter works on the calorimetric principle, which generates a thermo-emf, which is proportional to the thermal current generated in a calorimeter head under laser radiation [Lieberman A.A, High-precision calorimetric measuring detectors of intensity of laser radiation, Metrology, N9, 2002, Russia,].

4.2. Description of VNIIOFI measurement procedure

The comparison was carried out by means of calibration of a transfer detector – the laser power meter head OPHIR 10A provided by VNIIOFI.

At VNIIOFI the transfer detector was calibrated against the standard calorimeter PI-15 (National Primary Standard) by means of alternately measuring the laser beam power using the Primary standard system (Figure 2) described above. The calibration was done at two wavelengths: $0.532 \mu\text{m}$ and $1.064 \mu\text{m}$. The laser beam had diameter of 6 mm on the detector.

To minimize the uncertainty associated with the laser stability, monitor detectors were used to monitor the drift of the laser power during the calibration procedure. A silicon photodiode (marked as item 11 in Figure 2) was used as the monitor detector.

The measurement procedure was identical at every wavelength and is illustrated by a time diagram shown in Figure 3.

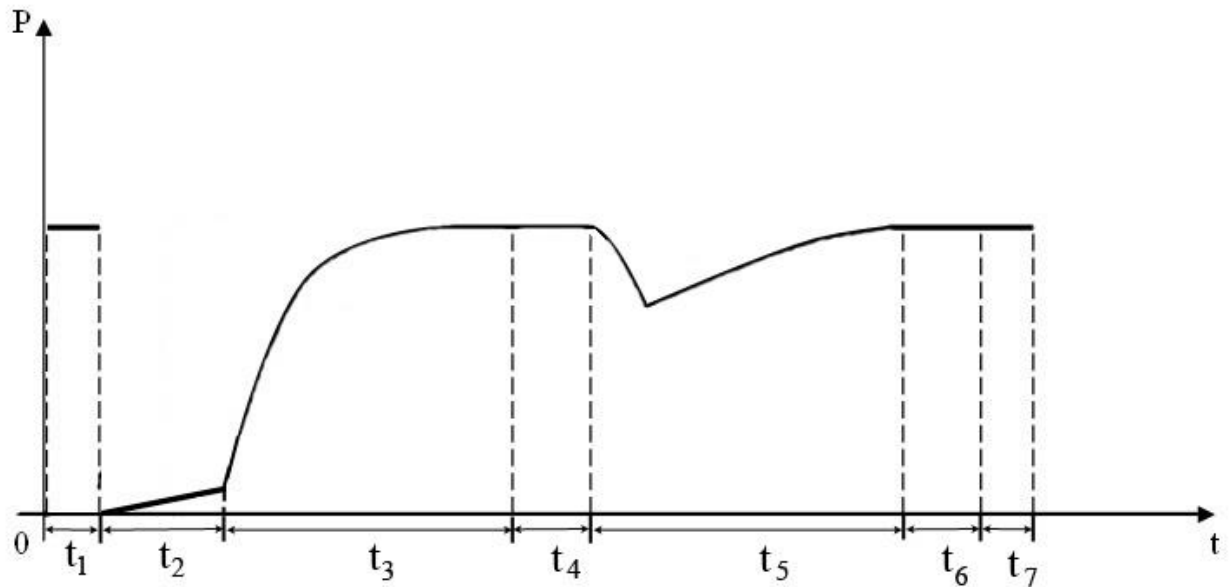


Figure 3. Time sequence of sampling periods during measurement where the y-axis indicates the injected power (laser or electrical) and the x-axis is time.

Figure 3 shows the time sequence diagram of measurements step by step: t_1 – evaluation of optical power by a monitor detector (30 s) - Laser injection only into monitor detector; t_2 – measurement of the zero level and drift by the calorimeter PI-15 (60 s, device 20 in Figure 2) – No injected power; t_3 – electrical substituting of the calorimeter (600 s) - Electrically injected power; t_4 – measurement of the electrical substitution power by the calorimeter (U, I, S) (120 s)- Electrically injected power; t_5 – exposure of the calorimeter with a laser beam (600 s) – Laser injection; t_6 – measurement of the laser power by the calorimeter PI-15 and monitoring of the laser power stability using a monitor detector during the calibration measurements – Laser injected power; t_7 – measurement of signals of the OPHIR 10A and monitoring of the laser power stability (the exposure time 30 s) – Laser injected power.

The exposure time was at least 30 s for the OPHIR 10A detector before reading the detector voltage. The offset voltage was also measured and subtracted.

The responsivity of the detector at each wavelength is determined as a ratio of the output voltage of the transfer detector to the laser power measured by the calorimeter PI-15.

The calibration measurement was performed 5 times for the transfer detector following the VNIIOFI normal procedure of calibration. The mean value and the standard deviations of the measurements are calculated.

The measurement was performed automatically by a computer controlled system, and the responsivity at a particular wavelength and power was calculated as:

$$s = \frac{U - U_0}{P_{st}}; \text{ where } U \text{ is the voltage (transfer standard readings); } U_0 \text{ is the offset voltage or}$$

zero level measured during time period t_2 (transfer standard readings), and P_{st} is the power measured by the calorimeter PI-15.

4.3. Laboratory conditions

The laboratory temperature and humidity during the calibration were (21 ± 1) °C and $(60 \pm 20)\%$, respectively. The transfer detector was kept at the laboratory conditions for more than one day before calibration.

4.4. Results of VNIIOFI measurements

4.4.1. VNIIOFI measurement of OPHIR 10A.

Table 4.3. Results of VNIIOFI 1-st measurement of OPHIR 10A (15 August 2013)

λ , μm	Power, W	Beam diam. mm	T °C	N of Meas	Responsivity s, mV/W	Standard unc. $U_c(s)$, %	k	Expanded unc. $U(s)$, %
0.532	1.00	6	20.8	5	0,5565	0,186	2,447	0,455
1.064	0.99	6	20.9	5	0,5640	0,118	2,145	0,253

Table 4.4. Results of VNIIOFI 2-nd measurement of OPHIR 10A (23 June 2015)

λ , μm	Power, W	Beam diam. mm	T °C	N of Meas	Responsivity s, mV/W	Standard unc. $U_c(s)$, %	k	Expanded unc. $U(s)$, %
0.532	1.00	6	21.2	5	0,5569	0,182	2,447	0,445
1.064	0.99	6	21.1	5	0,5636	0,122	2,160	0,263

4.4.2. Uncertainty budget

The uncertainty estimates for the VNIIOFI laser power measurements are presented following "ISO, Guide to the Expression of Uncertainty in Measurement", International Organization for Standardization, Geneva, Switzerland, 1993.

The Type A errors are assumed to be independent and normally distributed, with an uncertainty

$$u_A = \sqrt{\frac{\sum_{i=1}^n (x_i - \bar{x})^2}{n(n-1)}},$$

where \bar{x} is the mean value and n is the number of x_i values.

The Type B errors are assumed to be independent and have uniform distribution of width $2b$ and have an uncertainty of

$$u_B = \frac{b}{\sqrt{3}}.$$

The combined standard uncertainty is given as

$$u_C = \sqrt{u_A^2 + u_B^2}.$$

and the expanded uncertainty is

$$U(s) = k u_C,$$

where $k = t_{0,95}(v_{\text{eff}})$, $t_{0,95}(v_{\text{eff}})$ is the Student's coefficient for a 0,95 probability, and v_{eff} is the effective degrees of freedom given as

$$v_{eff} = (n - 1) \left[1 + \frac{u_B^2}{u_A^2} \right]^2,$$

where $n=5$.

Table 4.5. Uncertainty of standard calorimeter PI-15 (0.532 μm and 1.064 μm):

No	Uncertainty source	Degree of freedom	Type	Probability distribution	Standard uncertainty (%)
1	Voltage measurement on winding of the standard	∞	B	uniform	0,041
2	Voltage measurement on resistor of the standard	∞	B	uniform	0,029
3	Voltage measurement on thermobattery	∞	B	uniform	0,005
4	Absorption of the standard calorimeter	∞	B	uniform	0,017
5	Determination of the coefficient of equivalence of heat loss of the standard	∞	B	uniform	0,049
6	The correction of the temperature dependence of the standard	∞	B	uniform	0,017
7	The temperature dependence of the thermal source distribution	∞	B	uniform	0,029
	Type B total uncertainty			0.08	

Table 4.6. Uncertainty budget of VNIIOFI measurement of OPHIR 10A at a wavelength of 0.532 μm (15 August 2013)

No	Uncertainty source	Degree of freedom	Type	Probability distribution	Standard uncertainty (%)
1	Repeatability of standard calorimeter readings	4	A	normal	0,014
2	Repeatability of transfer standard readings (incl. zone nonuniform, laser stability, drift)	4	A	normal	0,162
3	Calibration of voltmeter	∞	B	uniform	0,01
4	Repeatability of monitor detector readings	4	A	normal	0,04
	Type A total uncertainty	0,167			
	Type B total uncertainty	0,080			
	Combined standard uncertainty	0,186			
	Effective degrees of freedom	6			
	Expanded uncertainty ($k = 2.447$)	0,455			

Table 4.7. Uncertainty budget of VNIIOFI measurement of OPHIR 10A at a wavelength of 1.064 μm (15 August 2013)

No	Uncertainty source	Degrees of freedom	Type	Probability distribution	Standard uncertainty (%)
1	Repeatability of standard calorimeter readings	4	A	normal	0,012
2	Repeatability of transfer standard readings (incl. zone nonuniform, laser stability, drift)	4	A	normal	0,075
3	Calibration of voltmeter	∞	B	uniform	0,01
4	Repeatability of monitor detector readings	4	A	normal	0,04
	Type A total uncertainty	0,086 %			
	Type B total uncertainty	0,080 %			
	Combined standard uncertainty	0,118 %			
	Effective degrees of freedom	14			
	Expanded uncertainty ($k = 2.145$)	0,253 %			

Table 4.8. Uncertainty budget of VNIIOFI measurement of OPHIR 10A at a wavelength of 0.532 μm (23 June 2015)

No	Uncertainty source	Degrees of freedom	Type	Probability distribution	Standard uncertainty (%)
1	Repeatability of standard calorimeter readings	4	A	normal	0,015
2	Repeatability of transfer standard readings (incl. zone nonuniform, laser stability, drift)	4	A	normal	0,158
3	Calibration of voltmeter	∞	B	uniform	0,01
4	Repeatability of monitor detector readings	4	A	normal	0,04
	Type A total uncertainty	0,164 %			
	Type B total uncertainty	0,080 %			
	Combined standard uncertainty	0,182 %			
	Effective degrees of freedom	6			
	Expanded uncertainty ($k = 2.447$)	0,445 %			

Table 4.9. Uncertainty budget of VNIIOFI measurement of OPHIR 10A at a wavelength of 1.064 μm (23 June 2015)

No	Uncertainty source	Degrees of freedom	Type	Probability distribution	Standard uncertainty (%)
1	Repeatability of standard calorimeter readings	4	A	normal	0,014
2	Repeatability of transfer standard readings (incl. zone nonuniform, laser stability, drift)	4	A	normal	0,081
3	Calibration of voltmeter	∞	B	uniform	0,01
4	Repeatability of monitor detector readings	4	A	normal	0,04
	Type A total uncertainty	0,091 %			
	Type B total uncertainty	0,080 %			
	Combined standard uncertainty	0,122 %			
	Effective degrees of freedom	14			
	Expanded uncertainty ($k = 2.160$)	0,263 %			

5. Measurement at NIST

5.1. Description of the measurement facility

The laser power meter was compared to NIST standard calorimeters at wavelengths of 0,532 μm and 1,064 μm (frequency doubled Nd:YAG and Nd:YAG laser). The laser beams had a nominal diameter of 5 mm on the detector surface, and the test detector was centered and normal to the incident beam. The power impinging upon the test instrument was measured concurrently using a calibrated beamsplitter and NIST standard calorimeters (see Figure 4). The beamsplitter ratio was calibrated for each data set using two NIST standard calorimeters.

Before the measurements began, the device under test (DUT) was allowed to reach equilibrium with the laboratory environment. Readings were recorded directly from the test detector. The calibration factor was then found by dividing the test instrument reading by the calculated incident power. The ambient temperature during these measurements was 22 \pm 1 $^{\circ}\text{C}$.

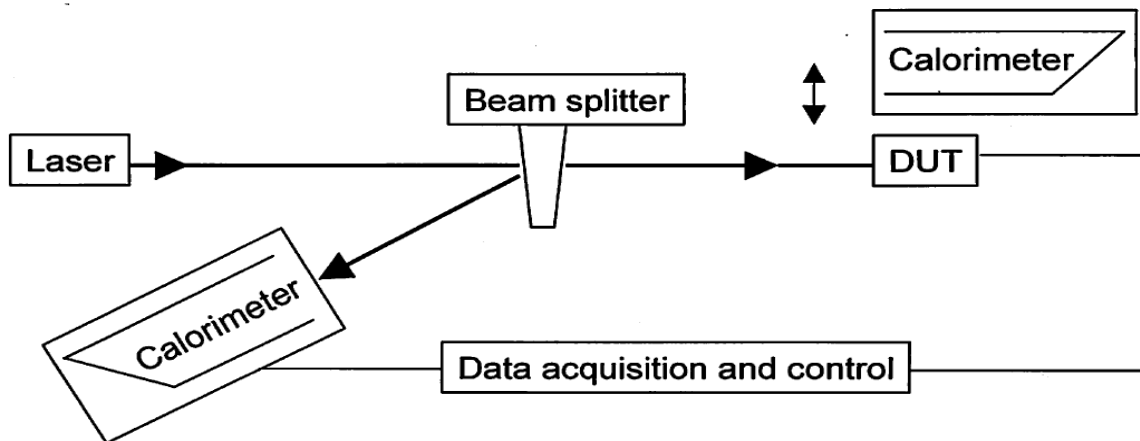


Figure 4. Measurement setup

5.2. Results of NIST measurements

5.2.1. NIST measurement of the OPHIR 10A.

Table 5.1. Calibration results (6 May 2014)

λ , μm	Nominal input power, W	N	Calibration factor, mV/W	Standard deviation, %	Expanded uncertainty ($k=2$), %
0,532	1,01	4	0,5582	0,02	$\pm 0,86$
1,064	1,01	4	0,5601	0,02	$\pm 0,86$

5.2.2. Uncertainty budget

The uncertainty estimates for the NIST laser energy measurements are assessed following guidelines given in NIST Technical Note 1297, "Guidelines for Evaluating and Expressing the Uncertainty of NIST Measurement Results" by Barry N. Taylor and Chris E. Kuyatt, 1994 Edition. To establish the uncertainty limits, the error sources are separated into Type B errors, whose magnitudes are determined by subjective judgment or other non-statistical method, and Type A errors, whose magnitudes are obtained statistically from a series of measurements.

All the Type B error components are assumed to be independent and have rectangular or uniform distributions (that is, each has an equal probability of being within the region, $\pm\delta_i$, and zero probability of being outside that region). If the distribution is rectangular, the standard uncertainty, σ_s , for each Type B error component is equal to $\delta_i/3^{1/2}$ and the total "standard deviation" is approximated by $(\sum\sigma_s^2)^{1/2}$, where the summation is performed over all Type B error components.

The Type A errors are assumed to be independent and normally distributed, and consequently the standard deviation, S_i , for each component is

$$S_r = \sqrt{\frac{\sum x^2 - \frac{(\sum x)^2}{N}}{N-1}},$$

where the x values represent the individual measurements and N is the number of x values used for a particular Type A error component. The standard deviation of the mean is $S_r / N^{1/2}$ and the total standard uncertainty of the mean is $[\sum (S_r^2 / N)]^{1/2}$, where the summation is carried out for all the Type A error components.

The expanded uncertainty is determined by combining the Type A and Type B "standard uncertainties" in quadrature and multiplying this result by an expansion factor of 2. The expanded uncertainty, U , is then

$$U = 2 \sqrt{\sum \sigma_s^2 + \sum \frac{S_r^2}{N}}$$

The values used to calculate the NIST uncertainties are listed in Table 5.2 for the power level tested.

The number of decimal places used in reporting the mean value of the calibration factor listed in Table 5.2 was determined by expressing the total NIST uncertainty to two significant digits.

Table 5.2 NIST measurement uncertainties for 0,532 μm and 1,064 μm wavelengths at 1 W

Source	Type B	Type A	
	δ_i	S_r	N
Standard calorimeter			
Inequivalence	0,15 %		
Absorptivity	0,01 %		
Electronics	0,10 %	0,10 %	30
Heater leads	0,01 %		
Window trans	0,11 %	0,02 %	6
Measurements			
Inject time	0,05 %		
Laser power drift	0,50 %		
Standard meter ratio	0,50 %	0,01 %	8
Transfer meter ratio		0,02 %	4
Relative expanded uncertainty ($k=2$)		0,86 %	

6. Results

6.1. Summary of participants' measurements results

Summary of participants' measurements results are presented in Table 6.1.

Table 6.1. Results of participants' measurements for OPHIR 10A

N	Date and Place	λ , μm	S_i , mV/W	Coverage factor k	Standard uncertainty $u_r(S_i)$, %	Relative Expanded Uncertainty, %
1	August 2013 VNIIOFI	0,532	0,5565	2,447	0,186	0,455
2	May 2014 NIST	0,532	0,5582	2,0	0,43	0,86
3	June 2015 VNIIOFI	0,532	0,5569	2,447	0,182	0,445
4	August 2013 VNIIOFI	1,064	0,5640	2,145	0,118	0,253
5	May 2014 NIST	1,064	0,5601	2,0	0,43	0,86
6	June 2015 VNIIOFI	1,064	0,5636	2,160	0,122	0,263

6.2 Comparison results

6.2.1 Artifact Stability

The (relative) standard uncertainty, associated with stability of the transfer detector during transportation is calculated as:

$$u_{tr}(S_i) = \frac{|\Delta_{rel}|}{2 \cdot \sqrt{3}} \quad (6.1)$$

where $\Delta_{rel} = \frac{(s_{after} - s_{before})}{\frac{1}{2}(s_{before} + s_{after})}$ is the relative change in the responsivity of detector head after

and before travel.

Results of calculations of $u_{tr}(S_i)$ are presented in Table 6.2.

Table 6.2. Results of calculation of $u_{tr}(S_i)$ for OPHIR 10A

λ , μm	0,532	1,064
Δ_{rel}	-0,072 %	0,071 %
$u_{tr}(S_i)$	0,0210 %	0,0205 %

For the OPHIR 10A power meter, the S_i values are calculated as an average between the first (Aug 2013) and the second (June 2015) VNIIOFI measurements:

$$S_i = \frac{S_{i2013} + S_{i2015}}{2} \quad (6.2)$$

6.2.2 Difference from Pilot

For each value of the artifact responsivity measured by a participant (S_i) there are two corresponding values measured by the pilot before and after the participant measurement.

The relative difference Δ_i of transfer standard responsivity between the participant (S_i) and the pilot (S_i^P) is then calculated by

$$\Delta_i = \frac{S_i}{S_i^P} - 1 \quad (6.3)$$

and its uncertainty $u(\Delta_i)$ by

$$u(\Delta_i) = \sqrt{u_r^2(S_i) + u_{tr}^2(S_i)} \quad (6.4)$$

The calculated results are summarized in Table 6.3, Table 6.4 and Fig. 5.

Table 6.3. Difference of transfer standard responsivity of participants from the pilot (%) and its uncertainty (532 nm)

Participant	S_i , mV/W	S_i^P , mV/W	$u_r(S_i)$, %	$u_{tr}(S_i)$, %	Δ_i , %	$u(\Delta_i)$, %
VNIIOFI	0,5567	0,5567	0,184	0,021	0	0,185
NIST	0,5582	0,5567	0,43	0,021	0,2694	0,4305

Table 6.4. Difference of transfer standard responsivity of participants from the pilot (%) and its uncertainty (1064 nm)

Participant	S_i , mV/W	S_i^P , mV/W	$u_r(S_i)$, %	$u_{tr}(S_i)$, %	Δ_i , %	$u(\Delta_i)$, %
VNIIOFI	0,5638	0,5638	0,12	0,0205	0	0,122
NIST	0,5601	0,5638	0,43	0,0205	-0,6563	0,4305

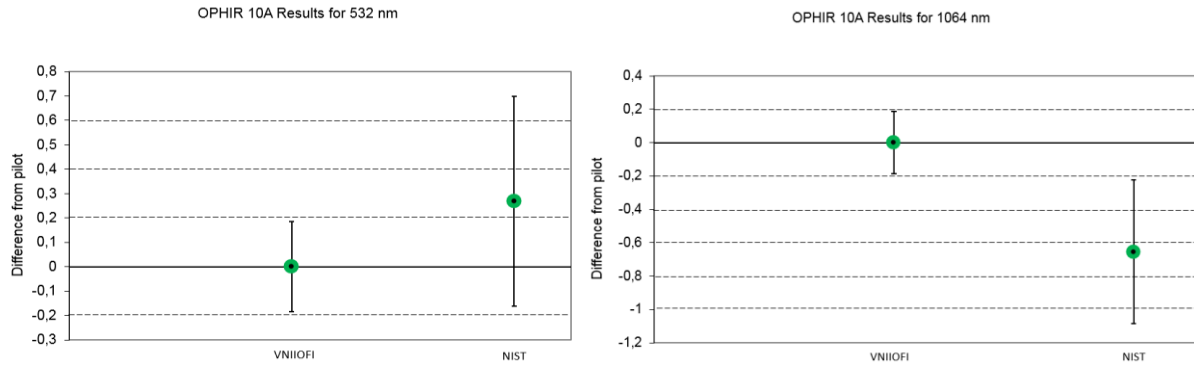


Figure 5. Difference of transfer standard responsivity of participants from the pilot (%) and its uncertainty.

6.3 Comparison Reference Values

The comparison Reference Value (RV) was calculated according to the Guidelines for CCPR Key Comparison Report Preparation (CCPR-G2, Rev.3, July 1, 2013).

At first, the cut-off value of the uncertainty is determined by

$$u_{cut-off} = average\{u_r(S_i)\} \text{ for } u_r(S_i) \leq median\{u_r(S_i)\} \quad (i = 0 \text{ to } N) \quad (6.5)$$

where N is the number of participants besides the pilot (i.e. $N = 1$).

Because there are only two participants, the cut-off uncertainty is the uncertainty of the participant with the lower uncertainty and an adjustment is not necessary.

The weights w_i is then calculated by

$$w_i = u_r^{-2}(\Delta_i) / \sum_{j=0}^N u_r^{-2}(\Delta_j) \quad (6.8)$$

Now the RV, Δ_{RV} , is determined by

$$\Delta_{RV} = \sum_{i=0}^N w_i \Delta_i \quad (6.9)$$

and the uncertainty of the RV is given by

$$u(\Delta_{RV}) = \sqrt{\sum_{i=0}^N \frac{u^2(\Delta_i)}{u_r^4(\Delta_i)}} / \sum_{i=0}^N u_r^{-2}(\Delta_i) \quad (6.10)$$

and the expanded uncertainty of the RV is $U(\Delta_{RV}) = ku(\Delta_{RV})$ ($k=2$).

The calculated values are summarized in Table 6.5 and Table 6.6 based on the summarized results in Table 6.3 and Table 6.4.

Table 6.5. RV and its uncertainty (532 nm), $u_{cut-off} = 0.307\%$

Participant	Δ_i , %	$u(\Delta_i)$, %	$u_r(S_i)$, %	w_i	Δ_{RV} , %	$U(\Delta_{RV})$, %
VNIIOFI	0	0,185	0,184	0,8439	0,042	0,17
NIST	0,2694	0,4305	0,43	0,1561		

Table 6.6. RV and its uncertainty (1064 nm), $u_{cut-off} = 0.275\%$

Participant	Δ_i , %	$u(\Delta_i)$, %	$u_r(S_i)$, %	w_i	Δ_{RV} , %	$U(\Delta_{RV})$, %
VNIIOFI	0	0,122	0,12	0,9260	-0,049	0,12
NIST	-0,6563	0,4305	0,43	0,0740		

6.4 Chi-square Value

The Chi-square value χ_{obs}^2 is calculated for consistency check by

$$\chi_{obs}^2 = \sum_{i=0}^N \frac{(\Delta_i - \Delta_{RV})^2}{u^2(\Delta_i)} \quad (6.11)$$

The calculated χ_{obs}^2 values are presented in Table 6.7

Table 6.7. Chi-square values

Wavelength	χ_{obs}^2	$\chi_{0,05}^2$	Consistency
532 nm	0,331	3.841	Satisfied
1064 nm	2,152	3.841	Satisfied

$\chi_{0,05}^2$, is determined from the Table 6.8, $v=1$.

For these comparisons for both wavelengths $\chi_{obs}^2 \leq \chi_{0,05}^2$, so the consistency is satisfied.

Table 6.8. Chi-square value (from the Guidelines CCPR-G2)

ν	$\chi^2_{0.05}(\nu)$
1	3.841
2	5.991
3	7.815
4	9.488
5	11.07
6	12.592
7	14.067
8	15.507
9	16.919
10	18.307
11	19.675
12	21.026
13	22.362
14	23.685
15	24.996
16	26.296
17	27.587
18	28.869

6.5 Differences from Reference Values

Difference from RV of the participant i is defined by

$$D_i = \Delta_i - \Delta_{RV}, \quad (6.12)$$

and the uncertainty of is given by D_i

$$u_i = \sqrt{u^2(\Delta_i) + u^2(\Delta_{RV}) - 2[1/\sum_{i=0}^N u^{-2}(\Delta_i)]}, \quad (6.13)$$

and

$$U_i = k u_i \quad (6.14)$$

with the coverage factor $k=2$ at the level of confidence of approximately 95 %.

Table 6.9 and 6.10 summarize the calculated differences from RV and uncertainties. These results are also presented in Fig. 6 and 7.

Table 6.9. Differences from RV and their uncertainties at $\lambda=532$ nm

Participant	$\lambda=532$ nm	
	$D_i, \%$	$U_i, \%$
VNIIOFI	-0,04207	0,146
NIST	0,22737	0,791

Table 6.10. Differences from RV and their uncertainties at $\lambda=1064$ nm

Participant	$\lambda=1064$ nm	
	$D_i, \%$	$U_i, \%$
VNIIOFI	0,049	0,066
NIST	-0,607	0,8284

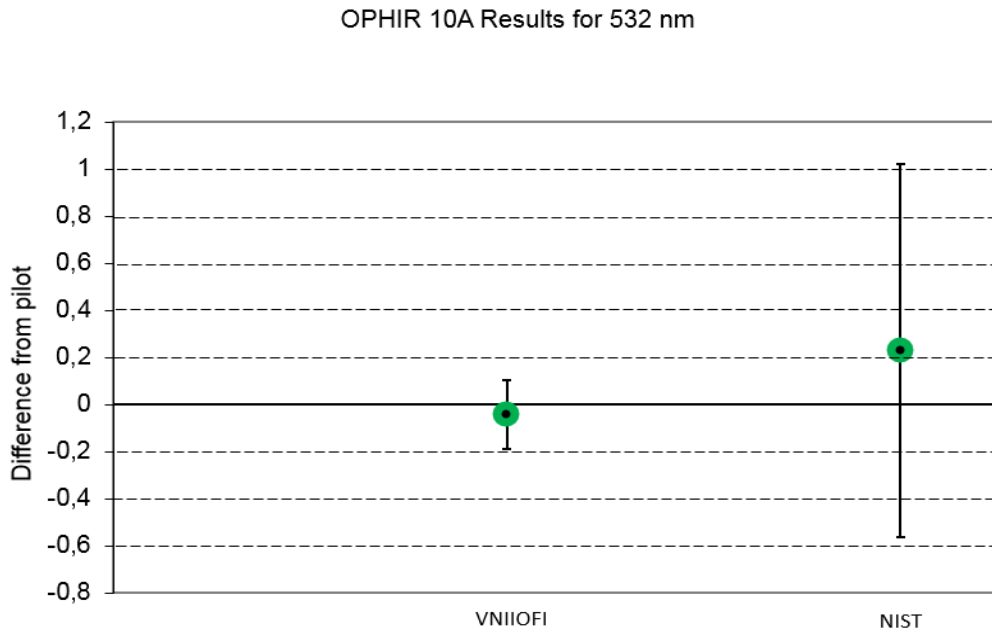


Figure. 6. Differences from RV (%) and expanded uncertainties of each participant at the wavelength of 532 nm.

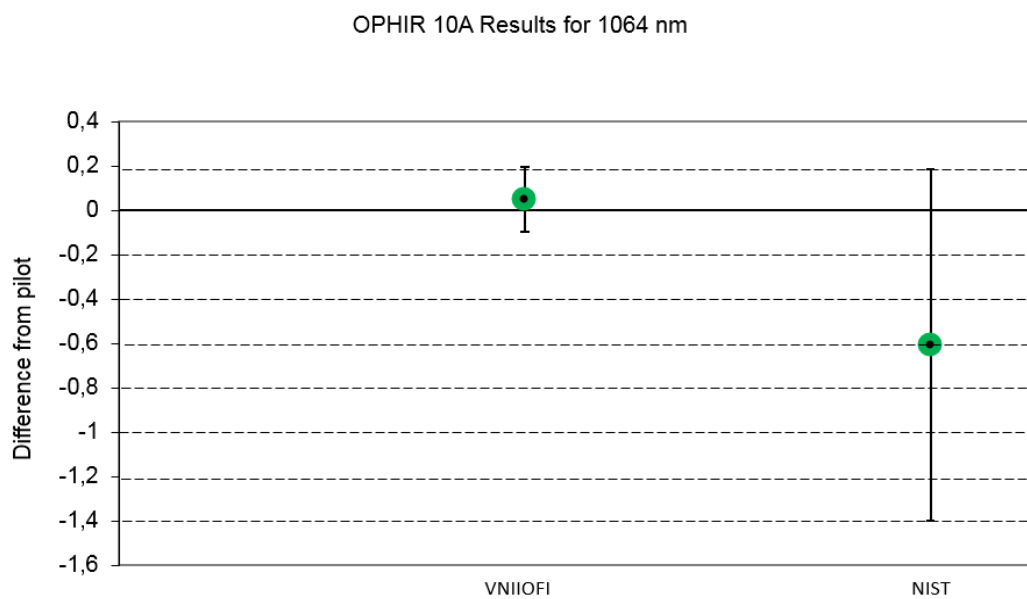


Figure. 7. Differences from RV (%) and expanded uncertainties of each participant at the wavelength of 1064 nm.

7. Conclusions

COOMET supplementary comparison of among NIST and VNIIOFI on power responsivity at optical power level of 1.0 W and at the wavelengths of 532 nm and 1064 nm has been carried out.

The comparison showed agreement between participants. Differences from the comparison Reference Values (RV) for all participants were within the RV expanded uncertainty.

With regard to CMC claim on the item 2.4.0 of CCPR service category that is "Responsivity, laser, power", this comparison report can be used to support it as an evidence.